Journal of Applied Polymer Science

Linear viscoelasticity, extensional viscosity, and oxygen permeability of nanocomposites based on propylene copolymer and organoclay

Verónica Riechert,[1,2] Lidia M. Quinzani,[1,2] Marcelo D. Failla[1,3]
[1]Planta Piloto de Ingeniería Química (PLAPIQUI), UNS-CONICET—Camino La Carrindanga km 7, Bahía Blanca 8000, Argentina
[2]Departamento de Ingeniería Química, Universidad Nacional del Sur (UNS)—Avenida Alem 1253, Bahía Blanca 8000, Argentina
[3]Departamento de Ingeniería, UNS—Avenida Alem 1253, Bahía Blanca 8000, Argentina
Correspondence to: M. D. Failla (E-mail: mfailla@plapiqui.edu.ar)

ABSTRACT: Random propylene-terpolymer (PEBC)/organophilic montmorillonite nanocomposites were prepared by melt mixing, using PEBC modified with maleic anhydride (PEBCg) as compatibilizer. Clay concentrations up to 8 wt %, compatibilizer/clay ratios up to 3:1 and concentrations of anhydride groups (AG) in PEBCg of 0.4 and 0.6 wt % were considered. The degree of exfoliation of the clay increases with PEBCg content and its concentration of AGs. The dynamic moduli allow estimating the percolation threshold of the nanofiller at 5.4 wt %, which yields an average of 11 silicate layers per tactoid at percolation, in agreement with the minimum thickness estimated from XRD data. The presence of exfoliated clay gives place to strain hardening and softening, depending on clay concentration and magnitude of the Hencky strain. The amount of exfoliated clay, however, plays a minor role in front of the content of AGs of the compatibilizer in regard with the oxygen permeability of the polymer. © 2017 Wiley Periodicals, Inc. J. Appl. Polym. Sci. **2018**, *135*, 45840.

KEYWORDS: clay; composites; polyolefins; rheology; structure-property relationships

Received 15 June 2017; accepted 25 September 2017
DOI: 10.1002/app.45840

INTRODUCTION

Random propylene copolymers (RPC) are produced by incorporation of ethylene or, less commonly, 1-butene or 1-hexene, to the reactor during polymerization reaction. The comonomers randomly substitute the propylene in the growing polymer chains, thus affecting the interactions of the monomer units and, therefore, the flow and final properties of the propylene homopolymer.[1] RPCs display better impact strength, especially at low temperatures, flexibility and optical properties than polypropylene (PP). Moreover, RPCs have lower melting point and specific gravity than PP. Due to its properties, RPCs are mostly used in applications that require good impact strength at low temperatures, some stiffness and transparency, and good moisture and gas barrier properties, like in food and medical packaging, and consumer goods. Moreover, many of these applications involve extensional flow during processing.[2] Thus, comprehend the response of RPCs under this type of flows is required.

On the other hand, a widely used method to enhance polyolefins properties is by the reinforcement with small amounts of high aspect ratio nanoparticles. This class of materials is known as polymer nanocomposites (PNCs), and they are expected to display improved fire retardant, mechanical, thermal, barrier, and electrical properties than the base polymer, preserving its transparency and low density.[3–5] Montmorillonite (MMT) is one of the nanofillers most used on the elaboration of PNCs due to the large surface-to-volume ratio, extraordinary intercalation/exfoliation capability, moderate charge density, and high cation exchange capacity.[3–5] MMT exists in nature in a tactoid structure comprised of several tens of aluminum-silicate stacked layers. In order to increase compatibility between polymer and filler, the inorganic cations present in the interlayer space of the clay are frequently exchanged for alquil-cations, obtaining an organophilic MMT (o-MMT). This process not only confers a more organophilic character to the clay but also increases the interlayer spacing facilitating the future exfoliation of tactoids and platelets and the intercalation of macromolecules.

Nanocomposites based on PP and o-MMT are analyzed in many publications,[5–7] and referenced works within. Several works also study nanocomposites based on RPC and o-MMT,[8–14] but only a few consider RPC with low comonomer content (<10 wt %).[10–14] These studies are based in composites having from 2 to 6 wt % of different o-MMTs and 1:1 to 3:1 compatibilizer/o-MMT ratios using maleated PP (PPg) and propylene copolymers. Although all these works analyze the structure of the nanocomposites, agreeing that they have exfoliated-intercalated structures. They consider just a few properties, that is, thermal,[11,13] mechanical,[11,14] and shear rheological properties.[14]

Both linear and nonlinear rheological properties of PNCs are very sensitive to their phase structure.[3–5] The elastic modulus and, in less extent, the viscous one are known to be increased by the presence of a nano or mesoscale structure of interacting particles. Furthermore, it has been generally observed that nanoparticles also increase the melt strength and induce strain hardening of molten PPs.[15–18] On the other hand, a few authors have reported a decrease of the melt strength of PP and/or strain softening at large strains.[16,19,20]

In a previous study, we have analyzed the thermal behavior of PNCs based on a random propylene-ethylene-butene copolymer (PEBC) using different concentrations of o-MMT and maleated PEBC (PEBCg).[21] The relation between morphology and the crystallization and thermal stability of the nanocomposites was investigated as a function of clay concentration, PEBCg:o-MMT ratio, and grafting degree of the compatibilizer. In this work, we analyze the linear viscoelastic behavior of these materials, as well as the response to start-up extensional flow. The information that can be obtained from this study is important for the comprehension not only of the structure–properties relationship of the PNCs but also of their processing behavior. The oxygen permeability of the nanocomposites, a key property in applications like packaging, is also analyzed.

EXPERIMENTAL

Materials

The polymer is a random propylene terpolymer from Petroquímica Cuyo S.A.I.C. (SP406) that contains 3 wt % of ethylene and 8 wt % of 1-butene (MFI = 6 g/10 min at 230 °C). The clay is a commercial o-MMT (Nanomer I.44 P from Nanocor, N44) with 2.6 nm of interlayer spacing containing dimethyl-dihydrogenated-tallow ammonium cations. The thermal degradation of the o-MMT begins at 200 °C.[21,22]

PEBC grafted with maleic anhydride (PEBCg) was used as compatibilizer in the elaboration of the nanocomposites. The PEBCg was synthesized by reactive mixing, using 2,5-dimethyl-2,5-di(*tert*-butyl peroxy)hexane as initiator. The first step in the modification consisted in impregnating the terpolymer with a solution of maleic anhydride dissolved in methyl ethyl ketone and then evaporating the solvent under nitrogen flow at room temperature. The impregnated polymer was then mixed with the initiator and incorporated into the mixer chamber of a Brabender Plastograph, where they were processed at 180 °C during 20 min under nitrogen flow. The modified polymer was then removed from the mixer and compressed to obtain ~3 mm thick specimens. Two compatibilizers were prepared as previously commented: PEBCg1, with a grafting degree of about 0.4 wt % of anhydride groups (AG), and PEBCg2, with about 0.6 wt %. The AG content of the compatibilizers was determined by Fourier transform infrared (FTIR) spectroscopy.[22] These concentrations of AG were chosen considering the reduction of the molecular weight produced by the functionalization process as the grafting degree increases, as it will be discussed further down.

Preparation of PNCs and Blends

The nanocomposites were elaborated by melt mixing the clay with the polymers (PEBC and PEBCg) at 180 °C in the discontinuous mixer during 20 min under nitrogen flow. A small amount of antioxidant Irganox1010 (0.01 wt %) was added to all polymers and composites. The clay was dried under vacuum at 130 °C during 24 h before mixing. After processing, the materials were removed from the mixer chamber with a spatula and rapidly compressed between aluminum plates to obtain ~3 mm thick specimens. Two groups of nanocomposites were obtained. One based on a 3:1 ratio of PEBCg1:o-MMT with different clay contents (2, 5, and 8 wt %), and another based on 5 wt % of clay and different ratios of PEBCg2:o-MMT (1:1, 2:1, and 3:1). A composite based on PEBC and 5 wt % of clay, and no compatibilizer, was also prepared. Table I displays the composition and identification code of all materials.

Polymer blends were also prepared under the conditions used for the composites. The proportion of the polymers in these

Table I. Composition of Nanocomposites and Blends

	Sample ID	PEBC (wt %)	Compatibilizer (wt %)	o-MMT (wt %)	PEBCg:clay	d_{001} (nm)
Composites	N2[a]	92	6	2	3:1	3.3
	N5[a]	80	15	5	3:1	3.3
	N8[a]	68	24	8	3:1	3.1
	N5-11[b]	90	5	5	1:1	3.2
	N5-21[b]	85	10	5	2:1	3.1
	N5-31[b]	80	15	5	3:1	3.2
	C5	95	-	5	—	3.3
Blends	m-N5[a]	84.2	15.8	—	Same ratio than in N5	
	m-11[b]	94.7	5.3	—	Same ratio than in N5-11	
	m-21[b]	89.5	10.5	—	Same ratio than in N5-21	
	m-31[b]	84.2	15.8	—	Same ratio than in N5-31	

Interlayer spacing corresponding to the (001) diffraction peak are included.
[a] Prepared with PEBCg1 (0.4 wt % AG).
[b] Prepared with PEBCg2 (0.6 wt % AG).

blends is equivalent to those used in the PNCs. Table I also displays the composition and identification code of these blends.

Characterization

Infrared spectra of all materials were collected using a Nicolet 520 FTIR spectrometer (Madison, WI, USA) on films of about 100 μm thickness, which were prepared by compression molding at 180 °C. This technique was used to verify the grafting of AGs in PEBC and to analyze potential chemical changes in the materials during processing. All characterized samples were previously subjected to vacuum at 110 °C during 24 h in order to eliminate possible unreacted maleic anhydride and secondary reaction products present in the compatibilizers. In the case of the PEBCg copolymers, the samples were previously purified, since the spectra were also used to quantify the grafting degree. This process consists in dissolving the polymers in hot xylene, precipitating them using methyl-ethyl ketone, and drying the materials under vacuum at 110 °C for 24 h.

The elastic (G') and viscous moduli (G'') of all materials were measured in a rotational rheometer (AR-G2, TA Instruments, New Castle, DE, USA) applying small amplitude oscillatory shear flow between parallel plates at 180 °C under nitrogen atmosphere. Disks of 25 mm diameter and 1.5 mm thick were cut from specimens previously molded using a hydraulic press at 180 °C. Dynamic stress sweeps were also performed to determine the stress range of linear response of each material and select the one to be used in the dynamic frequency sweeps. The effect of thermal annealing was analyzed by keeping selected samples of each material at 185 °C for 1 h under nitrogen atmosphere and then performing another dynamic frequency sweep.

The rotational rheometer equipped with the Sentmanat Extension Rheometer (SER) of Xpansion Instruments was used to measure the transient elongational viscosity, $\eta_E^+(\dot{\varepsilon},t)$, of the materials. Rectangular samples (18 × 10 × 0.7 mm in size) prepared by compression molding were tested at 150 °C under nitrogen atmosphere using three elongational rates, $\dot{\varepsilon} = 0.01$, 0.1, and 0.5 s^{-1}. The maximum Hencky strain (ε_{end}) allowed by the system is ~3.8, which determines a maximum testing time, $t_{end} = \varepsilon_{end}/\dot{\varepsilon}$, at each rate. In this work, we have chosen $\varepsilon_{end} = 3.5$.

The microstructure of the composites was studied by scanning electronic microscopy (SEM) using a LEO EVO-40 XVP equipment (Carl Zeiss AG, Oberkochen, Germany). This technique was selected due to its wide range of magnifications that includes sizes which allow analyzing the distribution and size of particles and tactoids. The analyzed surfaces were obtained with a cryo-ultramicrotome from the annealed specimens used in rheological characterization. The surfaces were chemically treated to enhance contrast between the clay and the polymer using a technique previously described.[22] The basal spacing of the filler was determined by X-ray diffraction (XRD) using a Phillips PW1710 diffractometer (Philips Corp., Westborough, MA, USA) equipped with a Cu-Kα radiation source of wavelength 1.54 Å operated at 45 kV and 30 mA. The diffraction spectra were recorded in the reflection mode over a 2θ range of 2°–40° in steps of 0.02° using a rate of 0.6°/min.

Oxygen permeability coefficients of all materials were measured at 23 °C with a MOCON Ox-Tran 2/21 equipment (Minneapolis, USA) following the ASTM Standard D3985 with gas pressure of 1 atm. The characterized films, which were obtained by compression molding at 180 °C, have exposed areas of 5 cm^2 and a thickness of 100–200 μm. Each reported permeability data corresponds to an average of at least four measurements.

When not specially indicated, the runs performed using the techniques described above were repeated using at least two different samples of each material to ensure reproducibility. Reported values of parameters or coefficients, like basal spacing, strain hardening coefficient, etc., correspond to the average of the measurements from those runs.

RESULTS AND DISCUSSION

Figure 1 shows two regions of the obtained infrared spectra of the polymers, blends and nanocomposites. The region between 1900 and 1550 cm^{-1} allows identifying the absorption bands associated to carbonyl groups, while the region between 1250

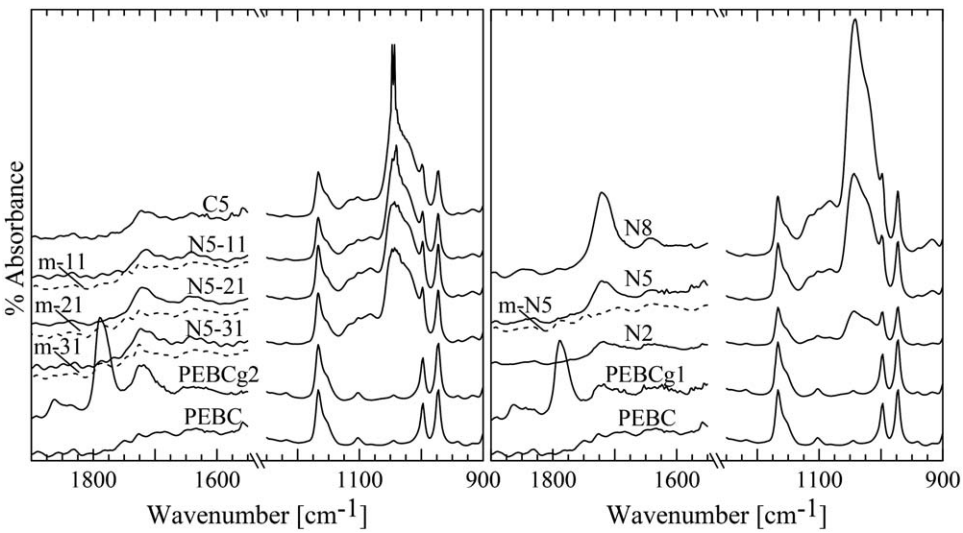

Figure 1. FTIR spectra of the polymers, blends, and composites. [Color figure can be viewed at wileyonlinelibrary.com]

and 900 cm^{-1} contains the overlapping bands corresponding to the Si—O—Si groups of the clay (centered at 1040 cm^{-1}). All spectra were normalized with the intensity of the band at 2720 cm^{-1}, that can be associated to the methylene groups of the macromolecule backbones, and arbitrarily shifted along the *y*-axis for legibility reasons. The maleated copolymers display a band at around 1790 cm^{-1} corresponding to the absorption of the carbonyl groups of the AG. The absorbance of this band was used to estimate the concentration of grafted anhydrides in PEBCg1 and PEBCg2, calculated as 0.4 and 0.6 wt %, respectively.[22] All blends, except m-11, also displays the band at 1790 cm^{-1} corresponding to the AG of the maleated copolymer. The absorbance of this band is proportional to the concentration of PEBCg2 in the blend. In the case of m-11, the low concentration of AGs makes not possible to distinguish this band.

Figure 1 also displays the FTIR spectra of the composites, where overlapping bands centered at 1040 cm^{-1} can be distinguished. As expected, the intensity of this band increases from N2 to N8, proportionally to clay concentration. The sensitivity of this band to the quality of intercalation/exfoliation of the clay in the nanocomposites can explain the different shapes observed in some spectra. According to Cole,[23] a broader band of smaller intensity signals a larger degree of intercalation/exfoliation of the clay. All composites analyzed in this study display similar degree of intercalation according to the d_{001} values listed in Table I, calculated from XRD presented in Riechert *et al.*[22] Consequently, the shapes of the band centered at 1040 cm^{-1} suggest the improvement of the degree of exfoliation with the presence of compatibilizer and with the augment of its concentration (see Figure 1, left).

It is interesting to notice that all composites also display absorption bands center at 1720 cm^{-1}. The absorption of this band, which can be associated to the presence of carbonyl groups, augments with the concentration of clay and compatibilizer in the 3:1 family of materials, and is practically constant in the compatibilized nanocomposites based on 5 wt % of clay. This behavior, together with the absence of a band at 1790 cm^{-1}, suggests that the AGs of PEBCg are consumed during mixing. Similar behavior has been observed in nanocomposites based on maleated compatibilizers, and has been associated to chemical reactions between the AGs of the compatibilizer and the surfactant of the o-MMT.[24–26] In fact, one of the reasons of the success of maleated compatibilizers in the preparation of nanocomposites may actually be the existence of these strong interactions, which may be helping to exfoliate the clay.

The images obtained by SEM displaying the phase structure of the compatibilized composites are exhibited in Figures 2 and 3. They reveal the presence of very small clay particles that are homogeneously distributed in the polymeric matrices. The size of the particles indicates that a high degree of clay exfoliation/disaggregation is achieved in all cases. The micrographs displayed in Figure 2 also show that the degree of exfoliation increases as the concentration of PEBCg2 augments for a constant concentration of clay, as already suggested by the infrared results. Undoubtedly, the increasing amount of maleated polymer improves the delamination of clay in tactoids, that is,

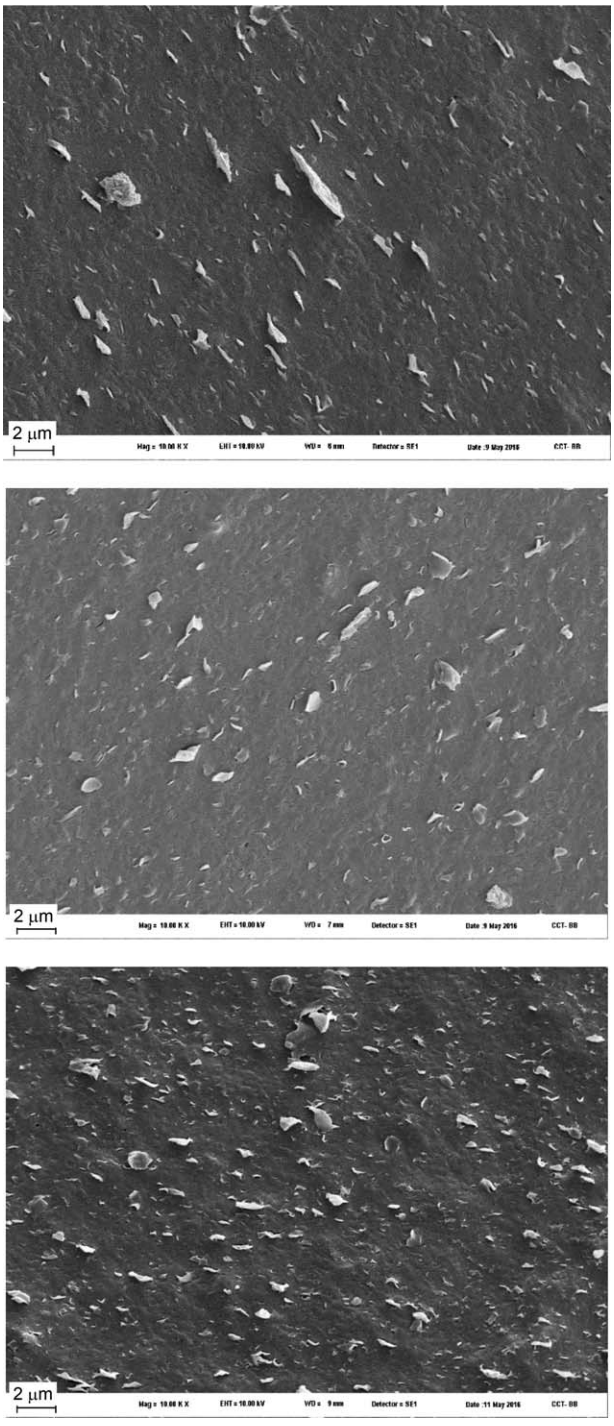

Figure 2. SEM micrographs of N5–11 (top), N5–21 (middle), and N5–31 (bottom) prepared with PEBCg2. Magnification 10,000×.

stacks of intercalated layers. Similarly, Figure 3 displays the SEM micrographs of nanocomposites based in different clay concentrations (2, 5, and 8 wt %) and a 3:1 ratio of PEBCg1:o-MMT. As expected, the amount of clay particles appreciated in the micrographs increases from N2 to N8. It can also be observed that the average size of the tactoids present in all of them is very similar, which implies that the clay particles were similarly disaggregated at all concentrations. The comparison of the

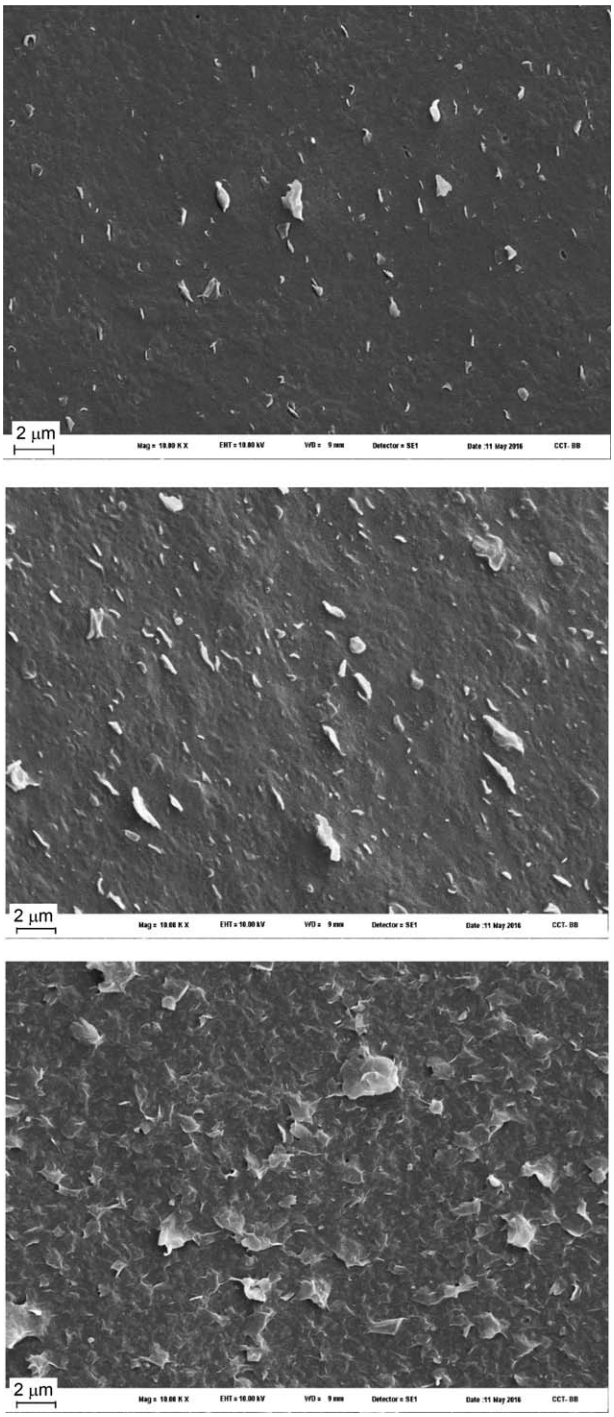

Figure 3. SEM micrographs of N2 (top), N5 (middle), and N8 (bottom) prepared with PEBCg1. Magnification 10,000×.

structure of N5–31 (Figure 2) with that of N5 (Figure 3) shows that the former presents a larger amount of smaller clay particles. As expected, the compatibilizer with a larger concentration of AG, PEBCg2, is more efficient in exfoliating the clay. It is also interesting to notice that the use of 8 wt % of o-MMT produces a percolated structure of clay platelets and tactoids. This can be observed in the closer view of the surface of N8 in Figure 4. It clearly shows the presence of very thin layers of

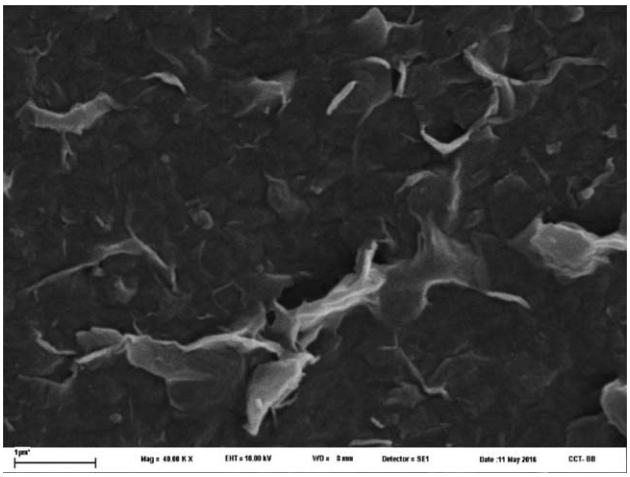

Figure 4. SEM micrograph of N8 obtained with a magnification of 40,000×.

stacked platelets that interact among them. Tactoids with a thickness smaller than 50 nm can be appreciated in the micrograph, which correspond to less than 16 layers of silicate.

The structural characterization of the materials was completed using XRD. Figure 5 shows the diffractograms corresponding to the pristine clay and selected nanocomposites: N2, N5, and N8 (based on PEBCg1), C5 (with no compatibilizer), and N5–31 (with 15 wt % of PEBCg2). The basal spacing of the d_{001} plane of the o-MMT, calculated by applying Brag's Law to the diffractograms of all PNCs, are listed in Table I. As it can be observed, the composites present a basal spacing of ~3.3 nm, which represents an increase of 0.5–0.7 nm in the separation between clay layers with respect to the pristine clay. Moreover, the value of d_{001} is practically independent of the composition, which means that the clay presents similar intercalated structure in all cases. As expected, as the filler concentration increases, the (001)

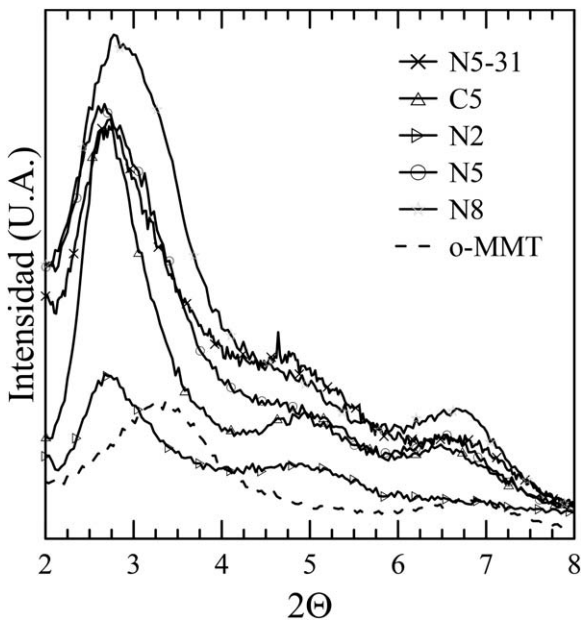

Figure 5. XRD diffractograms of the o-MMT, and some composites.

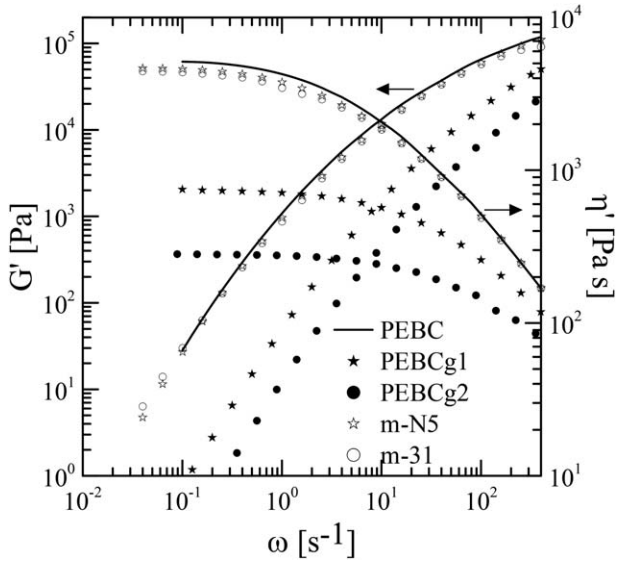

Figure 6. Elastic modulus and dynamic viscosity of the polymers and two blends, m-N5 and m-31, as a function of frequency at 180 °C.

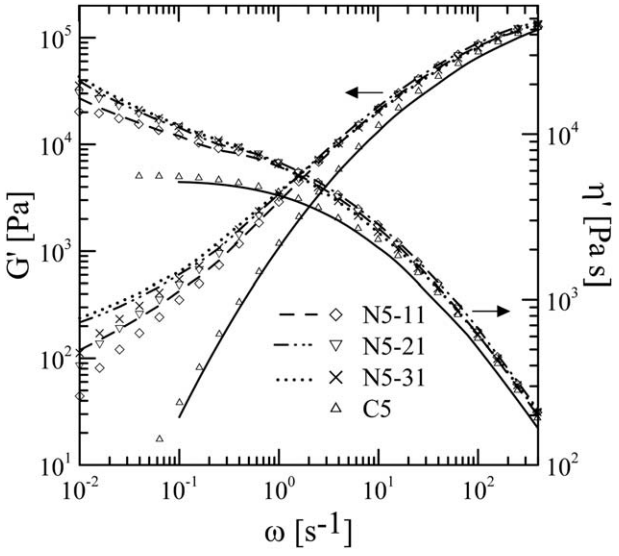

Figure 7. Elastic modulus and dynamic viscosity of composites based on 5 wt % of clay and different concentrations of PEBCg2, as a function of frequency at 180 °C. Full line, PEBC. Dashed lines, data after annealing.

plane peak increases in intensity, while those of N5 and N5–31 are very similar. In comparison, C5, which does not include compatibilizer, displays a narrower peak of higher intensity than the other composites based in 5 wt % of clay. This indicates that the compatibilized nanocomposites have a fraction of clay that has a very large basal spacing (2θ smaller than 2°) and/or it has been exfoliated, and that the stacking of the clay layers is less perfect in these materials. Together, SEM and XRD results show that all PEBC/PEBCg/o-MMT nanocomposites present intercalated/exfoliated structures and that the percolation threshold in the organization of clay tactoids is obtained with less than 8 wt % o-MMT, even when the PEBCg with the smallest concentration of AGs is used.

The elastic modulus, G', and dynamic viscosity, $\eta' = G''/\omega$, of the polymers measured at 180 °C are presented in Figure 6. The data of blends m-N5 and m-31 are included. All polymers have the typical rheological behavior of simple materials. PEBC has a zero-shear-rate viscosity, η_0, of 5100 Pa s and a terminal relaxation time, λ_0, calculated as $G'/\omega G''$ at $\omega \rightarrow 0$, of 0.6 s. Additionally, both η_0 and λ_0, of PEBCg1 and PEBCg2 are approximately 6.5 and 12 times smaller than those of PEBC, respectively. The smaller values of the rheological parameters of the compatibilizers basically reflect the reduction in molecular weight that occurs during the modification of PEBC. The attack of peroxide during the grafting reaction conduces to chain scission of the macromolecules and the consequent reduction in the average molecular weight.[1] In fact, PEBCg2, which contains the largest concentration of grafted AGs, displays the lower parameters. Assuming that the dynamic of PEBC and the grafted polymers is mainly affected by the size of their macromolecules rather by the chemical structure, a reduction in molecular weight of about 1.7 and 2 can be estimated considering the relation $\eta_0 \sim M_w^{3.4}$, which is applicable to lineal simple polymers.[2] With respect to the PEBC/PEBCg blends, they present rheological parameters that are smaller but close to those of PEBC. Figure 6 includes, as an example, the data of m–31 and m-N5. The dynamic moduli of the blends with lower concentrations of compatibilizer, m–11 and m–21, are located between those of PEBC and the displayed blends.

The dynamic moduli of the nanocomposites are presented in Figures 7 and 8. The data of PEBC are included in both figures as a reference. As it may be observed, all composites display parameters above the dynamic moduli of PEBC, mainly G' and at low frequencies. As the frequency increases, the moduli of the nanocomposites approach those of PEBC. In fact, at high frequencies, where the viscoelastic response is mainly due to the dynamic of short segments and small structures, the elastic and viscous moduli of all materials converge to similar values. The

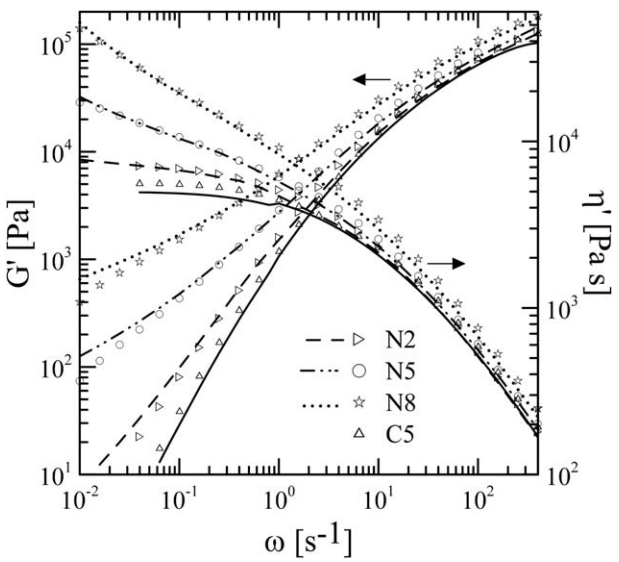

Figure 8. Elastic modulus and dynamic viscosity of composites prepared with different clay concentrations, as a function of frequency at 180 °C. Full line, PEBC. Dashed lines, data after annealing.

noncompatibilized composite, C5, is the one that has the smallest viscoelastic parameters, with moduli that are not far from those of the original PEBC. This behavior is typical of a microcomposite with a low content of filler. On the other hand, the larger dynamic moduli displayed by the compatibilized composites at low frequencies is the expected consequence in materials with important interactions between filler particles. The departure of the simple rheological behavior displayed by PEBC toward a solid-like behavior (G' that becomes similar or even larger than G'' at small frequencies) indicates that intercalated/exfoliated nanocomposites have been obtained.[5] This implies that PEBCg plays a crucial role in the formation of the nanocomposites.

In particular, Figure 7 displays the dynamic moduli of the composites based on 5 wt % of clay. As it may be observed G' and η' increase with the concentration of maleated copolymer. For example, the value of G' of fresh samples of the three compatibilized nanocomposites are about 100–500 times larger than in PEBC at the lowest frequency. This augment of the rheological parameters is due to the increase in frictional interactions among clay particles produced by the higher degree of exfoliation obtained as the concentration of PEBCg increases, as it was detected by SEM. Additionally, Figure 7 also displays the dynamic data measured after 1 h of annealing at rest at 185 °C under nitrogen flow (dashed lines). Both, the elastic modulus and the dynamic viscosity, undergo an increment after this treatment, keeping their relative original position. The augment is more noticeable in G', and mainly at low frequencies. For example, G' at 0.01 s^{-1} of the three nanocomposites increases about 2.5 times while η' augments ~10%. This behavior suggests that microstructural changes may be taking place during the annealing, resulting in higher degree of particle interactions.

Similarly, Figure 8 displays the dynamic data of the nanocomposites prepared with different concentrations of clay keeping a 3:1 ratio of PEBCg1/o-MMT. Both, G' and η' markedly increase with clay concentration, mainly at low frequencies, and even the use of 2 wt % of nanofiller produces a material with moduli that are larger than those of C5. Once again, the annealing process produces materials with larger dynamic parameters, mainly the elastic one. This effect is, however, less noticeable than in the materials prepared with PEBCg2. For example, N5–31 presents larger moduli than N5, and its moduli undergo a slightly larger increase after annealing (see Figure 7). This observation is in agreement with the larger degree of exfoliation detected by SEM in N5–31, which is based on the compatibilizer with a larger concentration of AGs.

Among the few studies that can be found in the literature based in RPC with low comonomer content (<10 wt %), only Liu *et al.*[14] analyze the rheological behavior of the materials. They consider nanocomposites based on RPC, 2 wt % of o-MMT, and 3 wt % of three different maleated copolymers. The obtained composites also present larger dynamic parameters than those of the RPC, but the differences that they observe are much smaller than the ones found in the PEBC system. For example, the maximum increment in the value of η_0 and G' at 0.01 s^{-1} observed by these authors is of ~20% and 300%, respectively. In the case of N2, the corresponding augments are ~50% and 700% (see Figure 8). Similar rheological behavior has also been found in the group while studying PNCs based in PP, a PPg, and different clays.[21,25] The dynamic data of these materials also augment with clay and compatibilizer concentration. However, the observed increments were smaller than the ones exhibited by the PEBC system when compared at equivalent concentrations. This occurs despite of using a compatibilizer with a higher content of AG (PPg with 1 wt %). However, in the analysis it has to be taking onto account the fact that the molecular weight of the PP is approximately 50% larger than the one of PEBC.

Another way of presenting the dynamic data is through the G''/G' ratio (=tan δ). This representation emphasizes the relative contribution of the elastic and viscous components in the rheological behavior. Figure 9 presents the values of tan δ corresponding to the dynamic data in Figures 7 and 8. As it may be observed, tan δ is, in general, larger than 1 ($G'' > G'$) but

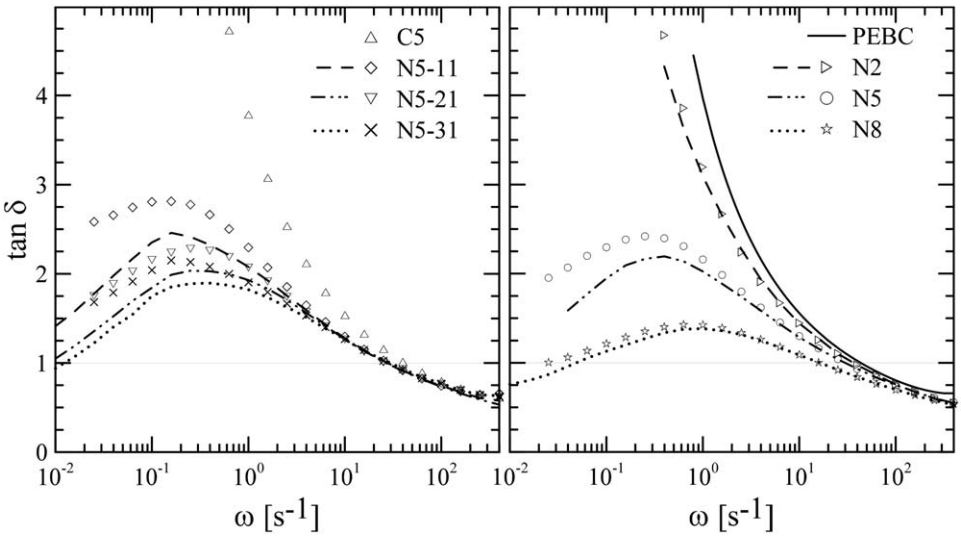

Figure 9. Tan δ as a function of frequency. Full line, PEBC. Dashed lines, data after annealing.

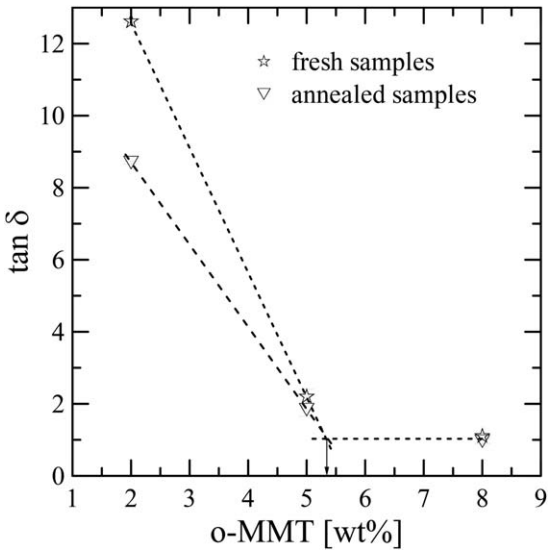

Figure 10. Estimation of the percolation threshold of nanocomposites based on PEBCg1.

approaches the value of 1, or it is even smaller, at low frequencies as the concentration of compatibilizer and/or clay augments. This is caused by the larger increase experienced by G' in relation with G'' at these conditions due to the augment in interactions between particles. It has been suggested that, beyond a critical volume fraction, the tactoids and individual layers of silicate are incapable of rotating freely and are prevented from complete relaxation when subjected to flow. This incomplete relaxation, due to the physical jamming or percolation, results in the presence of the pseudo-solid behavior observed in intercalated/exfoliated nanocomposites. In the case of the composites prepared with PEBCg2, those that reach solid-like behavior (tan δ ∼ 1 at low frequencies) are N5–21 and N5–31 after annealing. The other nanocomposites that present this rheological behavior are N5 (also after annealing) and N8 (even before annealing). This transition from liquid-like to solid-like performance suggests the formation of a three-dimensional superstructure of the exfoliated silicate layers and tactoids.[5] The tan δ data at low frequency can also be used to estimate the percolation threshold if plotted as a function of clay concentration.[26,27] Figure 10 displays the values of tan δ of N2, N5, and N8 measured at 0.04 s^{-1} before and after annealing. A significant change in behavior occurs at about 5 wt % of clay concentration in both set of data. In fact, the percolation threshold can be estimated with this methodology at 5.4 wt % of o-MMT.

Table II lists a series of studies that estimate the percolation threshold from rheological information in PE- or PP-based PNCs prepared by melt mixing using o-MMT and maleated PE (PEg) or PPg. Even though, molecular weight and processing conditions are two factors that may affect the degree of exfoliation of the clay, the results listed in Table II indicate that 5 wt % of o-MMT may be the minimum concentration for percolation if a 3:1 ratio of compatibilizer/clay is used with a compatibilizer with ∼1 wt % of AG. Percolation can be reached with less amount of clay using a larger amount of maleated polymer[28,29] or a compatibilizer with a larger concentration of AG.[27] Treece and Oberhause[33] have been able to produce a percolated structure using just 3 wt % of clay and 9 wt % of a

Table II. Representative Studies that Consider PNCs Based in PP or PE, o-MMT, and Maleated PP or PE, and Estimate the Percolation Threshold from Rheological Data

Reference	Polymer (MFI)[a]	Maleated compatibilizer[b] (AG content, MFI)	o-MMT	Percolation threshold[d]
Devendra *et al.*[28]	LLDPE (1.1 dg/min)	PEg (0.89 wt %, 1.8 dg/min)	N44	∼2 wt % (35:1)
Durmus *et al.*[27]	LLDPE (3.2 dg/min)	PEg (1.6 wt %, 4 dg/min)	C20[c]	∼3 wt % (3:1)
Tang *et al.*[29]	HDPE (6.5 dg/min)	PEg (0.85 wt %, 1.5 dg/min)	C20	∼2 wt % (11:1)
Horst *et al.*[26]	HDPE (8.0 dg/min)	HDPEg (0.17 wt %, <8 dg/min)	N44	∼9 wt % (2:1)
Galgali *et al.*[30]	PP (3.0 dg/min)	PPg (1 wt %, 140 dg/min)	C6[c]	∼6–9 wt % (1:1)
Gu *et al.*[31]	PP (3.8 dg/min)	PPg (0.8 wt %, 3.9 dg/min)	TJ4[c]	>7 wt % (4:1)
Lertwimolnun *et al.*[32]	PP (6.0 dg/min*)	PPg (1 wt %, 10 dg/min)	C20	∼5 wt % (4:1)
Rohlmann *et al.*[25]	PP (1.8 dg/min*)	PPg (1 wt %, 110 dg/min)	N44	∼5 wt % (3:1) ∼8 wt % (1:1) ∼12 wt % (1:8)
Treece and Oberhauser[33]	PP (12 dg/min*)	PPg (1 wt %, 110 dg/min)	C15[c]	∼3 wt % (3:1)
Bhattacharya *et al.*[17]	PP (3 dg/min)	PPg (1 wt %)	C20	∼6 wt % (1.5:1)
Present work	PEBC (6 dg/min)	PEBCg (0.4 wt %)	N44	∼5 wt % (3:1)

[a] MFI are reported at 190 °C/2.16 kg except when indicated with *, which correspond to 230 °C.
[b] The letter g in PPg and PEg stands for "maleic grafted" PP and PE, respectively.
[c] C20 and C6 refer to Cloisite 20A and Cloisite 6A [Southern Clays] which, as N44, are MMTs treated with dimethyl dehydrogenated tallow quaternary ammonium. N30 is Nanomer I.30P, from Nanoclor, modified with octadecylamine (ODA). TJ4 is a sodium MMT modified with dioctadecyl ammonium bromide.
[d] Clay concentration and compatibilizer/clay ratio are reported.

compatibilizer with 1 wt % of AG but after several hours of annealing at 180 °C or performing the rheological characterization at 210 °C (above the initial decomposition of the clay modifier). It is interesting to notice that in the case of the PEBC nanocomposites analyzed in the present work, the point of percolation is reached also at about 5 wt % of o-MMT when using a 3:1 ratio of compatibilizer/clay, but that in this case the maleated polymer has less than 1 wt % of AG.

From the estimated minimum concentration of o-MMT at percolation ($\omega_{per} = 0.054$), an average number of clay sheets in the tactoids at percolation can be estimated through the relation[34]

$$N_{per} = \frac{4}{3}\frac{R}{d_{001}}\frac{1}{\phi_{per,e}}\left[\frac{\omega_{per}\ \rho_{pol}}{\omega_{per}\rho_{pol}+(1-\omega_{per})\rho_{tact}}\right] \quad (1)$$

where ρ_{tact} (2.7 g/cm^3) and ρ_{pol} (0.78 g/cm^3) are the densities of the tactoids of o-MMT and the molten polymer, respectively[3]; R (500 nm) and d_{001} (3.2 nm) are the average radius and thickness of one layer of silicate, and $\phi_{per,e}$ (~0.3) is the critical volume fraction for percolation of spheres at random.[34] This equation assumes that all tactoids have identical number of clay layers (N_{per}), and that each tactoid occupies a spherical domain with a diameter equal to the lateral dimension of the platelets. The point of percolation of the PNC is then visualized as the percolation threshold of hypothetical spheres randomly distributed. Equation (1) yields an average number of ~11 silicate layers per tactoid at percolation threshold, which corresponds to an average thickness of 33 nm.

The minimum average thickness of the tactoids (L_{tact}) can also be estimated from XRD data using the formula credited to Sepehr *et al.*,[35]

$$L_{tact} = \frac{k\ \lambda}{\beta_{1/2}\ \cos\theta_B} \quad (2)$$

where $\beta_{1/2} \cong \theta_{max} - \theta_{min}$ and $\theta_B \cong (\theta_{max} + \theta_{min})/2$ are the peak width at half-maximum and the diffraction angle of the (001) reflection, λ is the wavelength of the radiation (0.154 nm), and $k = 0.94$.[34,35] For example, from the diffractogram of N5, $\beta_{1/2}$, and θ_B have values of ~0.01 and ~0.03 rad, respectively, estimated with respect to the baseline. For the nanocomposites of the present work, eq. (2) yields a minimum average thickness of the tactoids of ~15 nm, which is in concordance with the average size calculated from rheology data.

As already commented in the Introduction, the rheological characterization of the materials included the measuring of the

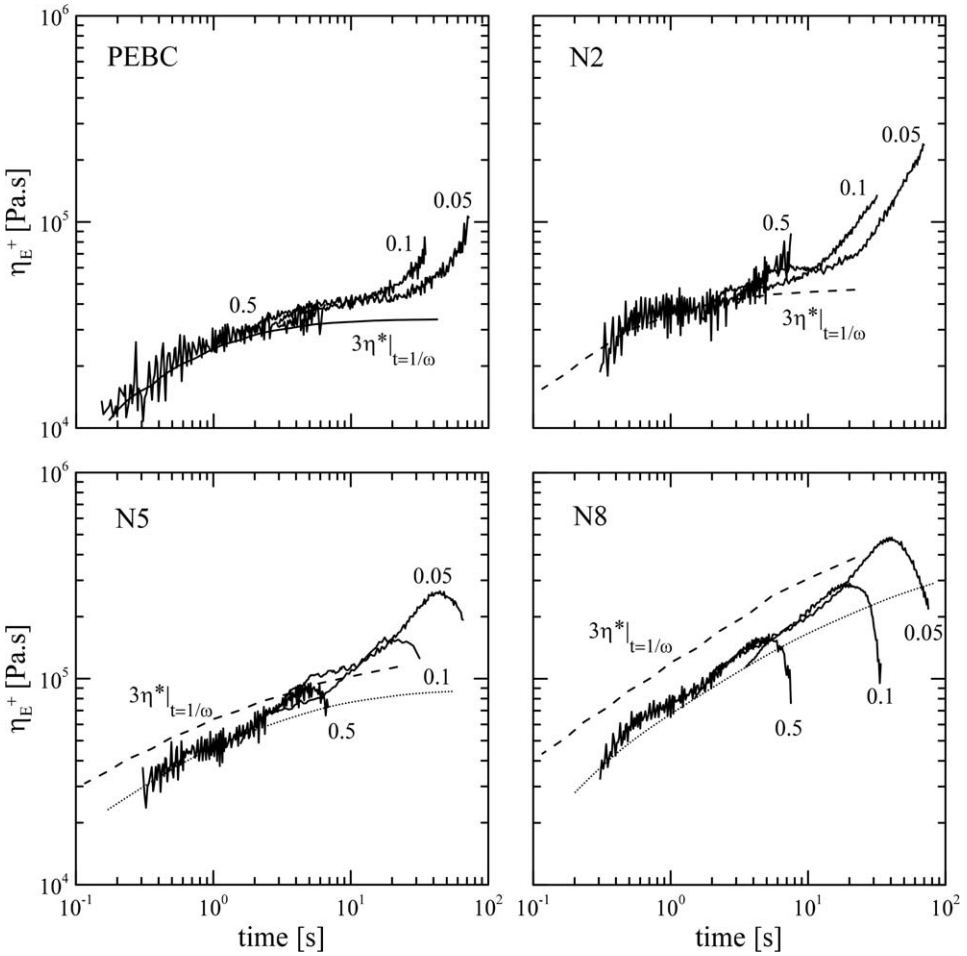

Figure 11. Transient extensional viscosity of PEBC, N2, N5, and N8 at 150 °C and different extensional rates. Dashed lines, estimated position of 3η* at 150 °C. Dotted lines, linear envelopes.

Table III. Strain Hardening Coefficient (SH) of Some Materials

	SH for $\dot{\varepsilon}_0 = 0.05\ s^{-1}$		SH for $\dot{\varepsilon}_0 = 0.1\ s^{-1}$	
	At t_{max}	At $t_{end} = 70$ s	At t_{max}	At $t_{end} = 35$ s
PEBC	—	3.3	—	2.1
N2	—	5.2	—	3.3
N5	2.7 ($t_{max} = 43$ s)	1.8	1.8 ($t_{max} = 20$ s)	1.1
N8	1.3 ($t_{max} = 40$ s)	0.77	1.3 ($t_{max} = 20$ s)	0.56

transient extensional viscosity, $\eta_E^+(\dot{\varepsilon},t)$, at elongational rates $\dot{\varepsilon} = 0.01$, 0.1, and 0.5 s^{-1}. Figure 11 displays the data of PEBC, and the three PNCs prepared with different clay concentrations. The data of the complex viscosity, plotted as $3\eta^*$ at $t = 1/\omega$, are included for comparison. η^* corresponds to $G^*/\omega = (G'^2 + G''^2)^{1/2}/\omega$. The linear viscoelastic data from shear flow are expected to agree with the "envelope curve" formed by the linear response of the material in extensional flow, η_{E0}^+ (for very small deformations or slow elongational rates)[2]

$$\lim_{\dot{\varepsilon}\to 0} \eta_E^+(\dot{\varepsilon},t) = \eta_{E0}^+ = 3\eta^*(\text{at } t = 1/\omega) \quad (3)$$

The $3\eta^*$ data included in Figure 11 were calculated from the dynamic moduli in Figures 6 and 8, which have been shifted to 150 °C using a time–temperature shifting coefficient (a_T) of 2.19. This coefficient was determined for PEBC while building master curves of the dynamic moduli from data measured between 150 and 190 °C using annealed samples. The fitting of the calculated a_T coefficients to the Arrhenius model gives a flow activation energy for PEBC of 42 kJ/mol, which is similar to the flow activation energy of PP.[3,36] The a_T of 2.19 was also used to shift the dynamic data of the nanocomposites from 180 to 150 °C. This is an adequate procedure for PNCs as in the presence of clay it is not expected to affect the thermorheological behavior of the polymeric matrix.[3,25,30] However, an increasing amount of functionalized polymer in the PNCs might gradually change the activation energy of the polymeric matrix. The position of the $3\eta^*$ data of the PNCs, which have been signaled by dashed lines in Figure 11, should then be considered approximate (mainly in the case of N5 and N8). As expected, the results in Figure 11 show that the envelope curve of PEBC, and even that of N2, overlaps with the data of $3\eta^*$. However, as the concentration of clay increases, η_{E0}^+ separates from $3\eta^*$, albeit the curves remain practically parallel. The approximate value of a_T used to shift the dynamic data may be the cause of this effect.

The data in Figure 11 also show that, as the Hencky strain increases, the elongational viscosity of PEBC rises above the linear data. The strain hardening displayed by the polymer, even if small, may be due to the existence of a small degree of long-chain branching or a small fraction of very large molecular weight material.[2] It is interesting to notice that the time of the departure of the data from the envelope curve, which decreases as the deformation rate augments, determines a Hencky strain that is practically constant ($\varepsilon = \dot{\varepsilon}_0 t = 1.2$–1.5).

The results in Figure 11 also show that the addition of clay produces not only a quantitative change in the extensional viscosity but also a qualitative one. In the linear regime, the position of the envelope curves reveal that the extensional viscosity augments with the incorporation of clay, and that the time of the departure of the data from the envelope curves occurs always at Hencky strains close to 1.2–1.5. Once the flow begins to affect the network structure of macromolecules and clay tactoids as well as their conformations, strain hardening appears that is followed by a noticeable strain softening at large strains in the nanocomposites with larger concentrations of o-MMT. Table III displays the values of a strain hardening coefficient (SH) define as,

$$\text{SH} = \frac{\eta_E^+(\dot{\varepsilon},t)}{\eta_{E0}^+(t)} \quad (4)$$

which has been calculated at two testing times: the final one, t_{end}, at maximum Hencky strain, and the one corresponding to the position of the maximum elongational viscosity, t_{max}.

According to the results in Figure 11, N2 displays strain hardening at all deformation rates. Moreover, the values of SH at t_{end} summarized in Table III indicate that the addition of 2 wt % of o-MMT produces a strain hardening that is ~60% larger than that of PEBC. Strain hardening can also be appreciated in N5 and N8, which is followed by strain softening. As it is shown by the values of SH, the strain hardening decreases with the augment of clay content and/or elongation rate. On the other hand, the strain softening that appears at large Hencky strains becomes more important as the clay concentration increases. Moreover, SH at t_{end} in the case of N8 reaches a value that is even smaller than 1, which means that in this material η_E^+ reaches a value that is lower than the corresponding to the linear envelope. Additionally, it is interesting to notice that the strain at which the maximum elongational viscosity occurs in N5 and N8 ($\varepsilon_{max} = \dot{\varepsilon}_0 t_{max}$) is approximately the same at the three elongational rates, with a value of ~2.

To complete the analysis, the transient extensional viscosity of the rest of the materials based on 5 wt % of o-MMT was measured at 0.1 s^{-1}. Figure 12 shows those results, as well as the superposition of the data of the materials shown in Figure 11. The addition of 5 wt % of clay, without the presence of compatibilizer, does not change the extensional viscosity of PEBC. On the other hand, all PNCs based in 5 wt % of clay display larger extensional viscosity than PEBC that, as it was observed in the

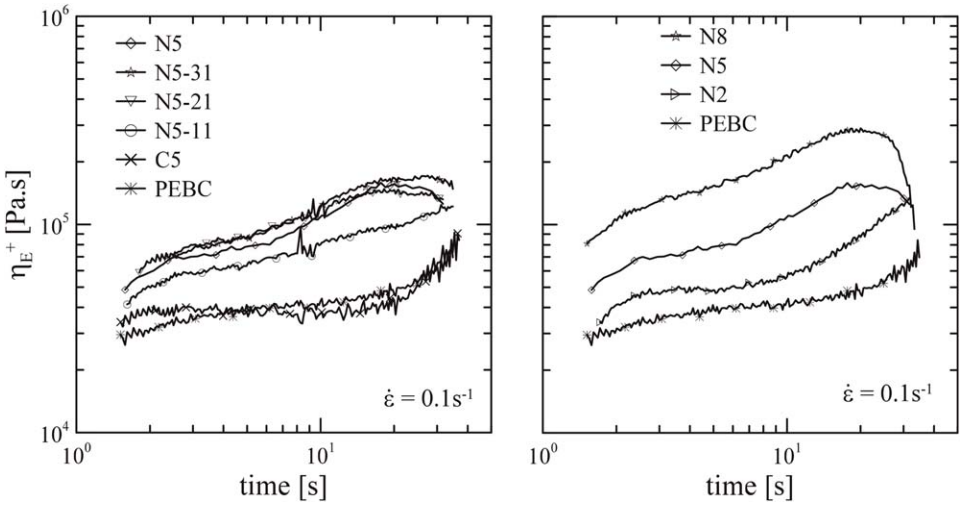

Figure 12. Transient extensional viscosity of all materials measured at 150 °C and 0.1 s^{-1}.

dynamic data, gradually increases with the content of compatibilizer. Furthermore, as the disaggregation of the clay improves with the addition of larger concentrations of compatibilizer, strain softening develops at large strains, which is not present, for example, in N5–11. The superposition of the data of PEBC, N2, N5, and N8 at a given elongational rate clearly show the augment in elongational viscosity in the linear regime (even with just 2 wt % of clay) and the substantial strain softening that develops at large Henchy strains as the clay concentration augments. Summarizing, it may be concluded that the presence of clay changes the behavior of the polymer under extensional flow only if it reaches a large degree of exfoliation, and that the effect of the interactions between particles becomes more noticeable as the clay concentration and/or the disaggregation of the clay increases. As it was already commented, the tactoids constitute a tridimensional network in the polymeric matrix of N8, and are near percolation in N5. This tridimensional network is responsible of the augment in the linear viscoelastic parameters, both in shear and elongational flow. However, when the network is deformed by the flow, at $\varepsilon > 1.2$–1.5, the degree of interactions between particles may be reduced by deformation and orientation of the relatively flexible tactoids. Moreover, the displacement and deformation of the tactoids by the flow may impose some shear flow in the polymer surrounding the filler particles, reducing the extensional deformation of the macromolecules and contributing to the observed decrease in viscosity at large Hencky strains.[19,20]

One property that may be improved by the presence of nanofillers is the gas permeability. Figure 13 displays the oxygen permeability coefficients measured using compressed-molded films of fresh materials (as they come from the mixer). The polymer, PEBC, has a coefficient of 112 cm^3 mm/m^2 day atm. This value practically doubles most reported permeability coefficients of isotactic PP (which is about 65 cm^3 mm/m^2 day atm).[37–39] This behavior may be due to differences in the crystal structure and degree of crystallinity between both types of polymers.[40] In fact, PEBC has a degree of crystallinity (X_c) calculated from the enthalpy of crystallization (ΔH_c) of about 34%,[22] which is lower than the X_c of most isotactic PPs.[37,39,41]

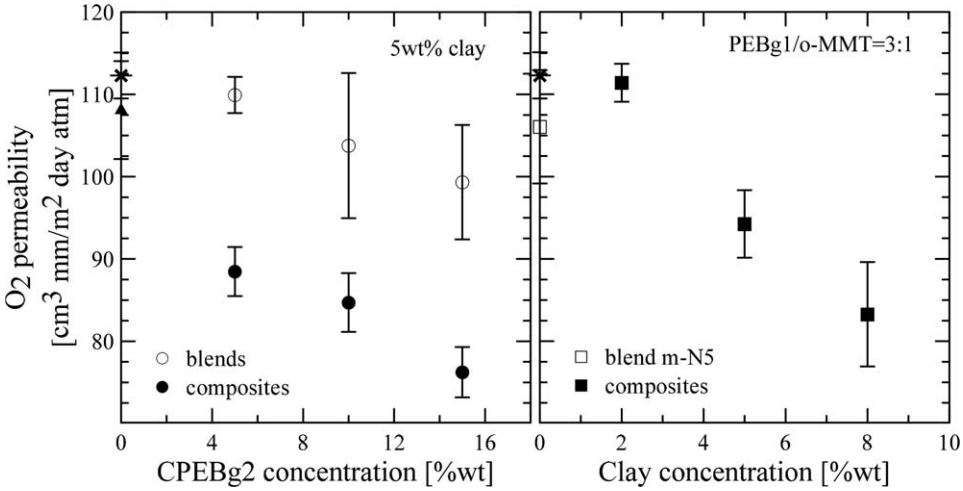

Figure 13. Oxygen permeability of PEBC (×), C5 (▲), and blends and nanocomposites based in PEBCg2 (left) and PEBCg1 (right).

The addition of maleated copolymer to PEBC decreases its oxygen permeability. Among the analyzed blends, m-31 displays the lowest value of permeability, which is 12% smaller than that of PEBC. A similar trend has been observed in blends of PP or PE and their corresponding maleated polymers, although the reduction displayed by blends with up to ~15 wt % of compatibilizer, like those considered in this study, is generally smaller.[26,37,39,42] As it was shown in the previous article,[22] all the analyzed blends have similar degrees of crystallinity, and therefore, the observed decrease in permeability may be explained by variations in the concentration of AGs in the amorphous phase, thus affecting the permeation process of the gas molecules. This conclusion is sustained also by the larger permeability of m-N5 compared with m-31, being m-N5 based in the compatibilizer with smaller concentration of AGs.

The addition of 5 wt % of clay to PEBC produces a marginal decrease in permeability (see the data of C5), as expected for microcomposites with low filler concentration. On the other hand, the incorporation of the compatibilizer, PEBCg2, produces nanocomposites with oxygen permeability coefficients smaller than those of PEBC and even the corresponding blends (Figure 13, left). The minimum value, which is displayed by N5–31, is 32% and 23% smaller than those of PEBC and the blend m-31, respectively. Moreover, the permeability of the nanocomposites prepared with PEBCg1 (Figure 13, right) decreases with clay concentration, being N8 the one that displays the minimum value (26% smaller than that of PEBC). It is interesting to notice that N5–31 displays the lowest permeability, even lower than N8. Two effects might be contributing in generating this behavior. One is the presence of the exfoliated clay, which introduces tortuous diffusion path for the permeation of the gas molecules,[40] and the other is the chemical nature of the components and of those substances that may result from the reaction that involve the AGs and the clay modifier (as suggested by FTIR results). Surely, N5–31 displays the largest reduction in the permeability of PEBC due to the combination of both effects. It is interesting to notice that N8 has larger oxygen permeability in spite of having greater concentrations of both clay and compatibilizer. Certainly, the larger concentration of AGs and lower molecular weight of the compatibilizer used in the synthesis of N5–31 is the key for its enhanced permeation barrier.

The observed reduction in oxygen permeability when using 5 wt % of clay is similar to that detected by other authors while studying PP or PE based nanocomposites. Although there are several factors that may contribute to determine the diffusion rate of oxygen molecules through polymeric films (as temperature, relative humidity, type of clay and compatibilizer, polymer crystallinity, etc.), most of these authors have observed about 30%–40% reduction in oxygen permeability when using 5 wt % of o-MMT and 5–15 wt % of maleated compatibilizer with 0.7–1 wt % of AGs.[43–45] Horst *et al.*[26] observe a reduction of just ~11% in the permeability of a HDPE when using 10 wt % of a PEg with 0.17 wt % of AGs. Once again, all considered, it can be concluded that the affinity and consequent interactions between compatibilizer, clay and clay surfactant, is, together with the component concentrations, the most important factor in determining gas diffusion.

CONCLUSIONS

Nanocomposites were prepared by melt mixing a random PEBC with o-MMT. Maleated PEBC was used as compatibilizer. The PEBCg was synthesized by reactive grafting MA onto the terpolymer on the molten state. Two compatibilizers were obtained in this way, with different grafting degree and molecular weight.

According to FTIR, SEM, and XRD results, all compatibilized composites display intercalated/exfoliated structure. Moreover, the infrared results suggest that, during the mixing process, a chemical reaction takes place between the AGs of the compatibilizer and the o-MMT, probably its surfactant. Furthermore, according to rheological and SEM data, the compatibilizer plays a key role in the degree of exfoliation/delamination of the clay during processing. The increase of the dynamic moduli, mainly the elastic one, at low frequencies, which is indicative of strong interactions between filler particles, demonstrates that the use of a compatibilizer with larger concentration of AGs and lower molecular weight favors the exfoliation/disaggregation of the clay. The extensional viscosity in the linear regime is similarly affected by the clay and its state of exfoliation. However, at large Hencky strains, a gradual change from strain hardening to strain softening occurs as the clay concentration increases. This phenomenon indicates that the flow affects the degree of interaction among particles and/or that the deformation of the tactoids interferes with the flow of the polymer chains around them.

In agreement with estimations from XRD data, the dynamic moduli of nanocomposites prepared with different clay concentration suggest that the percolation threshold of the nanofiller is about 5.4 wt %, when using the PEBCg with lower content of AGs. This value remains the same when calculated from rheological data measured after the nanocomposites are subjected to 1 h of annealing at 185 °C, even though this process induces further changes in the structure that result in higher degree of interactions between particles.

The addition of 5 wt % of clay, without compatibilizer, produces a marginal reduction in the oxygen permeability of PEBC. The nanocomposites, however, display lower permeability, which decreases with either clay or compatibilizer concentration. The use of the compatibilizer with the largest concentration of AGs and lower molecular weight gives place to the largest decrease in permeability. The role of the grafting degree of the compatibilizer is so important that to achieve similar permeability values, for a given clay concentration, the amount of PEBCg1 (0.4 wt % of AG) should at least triplicate that of PEBCg2 (0.6 wt % of AG).

ACKNOWLEDGMENTS

The authors acknowledge the National Research Council of Argentina (CONICET), the Universidad Nacional del Sur (UNS), and the Agencia Nacional de Promoción Científica y Tecnológica (ANPCyT) for the support of this project.

REFERENCES

1. Gahleitner, M.; Paulik, C. In Brydson's Plastics Materials; Gilbert, M., Ed.; Elsevier: Kidlington, UK, **2017**; Chapter 11, p 279.
2. Dealy, J. M.; Wang, J. Melt Rheology and its Applications in the Plastics Industry; Springer: Dordrecht, the Netherlands, **2013**.
3. Utracki, L. A. Clay-Containing Polymeric Nanocomposites; Rapra Technology Limited: Shrewsbury, UK, **2004**.
4. Mittal, V. *Materials* **2009**, *2*, 992.
5. Sinha Ray, S. Clay-Containing Polymer Nanocomposites: From Fundamentals to Real Applications; Elsevier: Great Britain, UK, **2013**.
6. Chrissopoulou, K.; Anastasiadis, S. H. *Eur. Polym. J.* **2011**, *47*, 600.
7. Pandey, J. K.; Reddy, K. R.; Mohanty, A. K.; Misra, M. Handbook of Polymer Nanocomposites. Processing, Performance and Application; Springer-Verlag: Berlin, **2014**; Vol. A.
8. Kumar, A. P.; Singh, R. P. *J. Appl. Polym. Sci.* **2007**, *104*, 2672.
9. Passaglia, E.; Bertoldo, M.; Ciardelli, F.; Prevosto, D.; Lucchesi, M. *Eur. Polym. J.* **2008**, *44*, 1296.
10. Preschilla, N.; Sivalingam, G.; Abdul Rasheed, A. S.; Tyagi, S.; Biswas, A.; Bellare, J. R. *Polymer* **2008**, *49*, 4285.
11. Palza, H. *Macromol. Mater. Eng.* **2010**, *295*, 492.
12. Prevosto, D.; Lucchesi, M.; Bertoldo, M.; Passaglia, E.; Ciardelli, F.; Rolla, P. *J. Non-Cryst. Solids* **2010**, *356*, 568.
13. Liu, B.; Shangguan, Y.; Zheng, Q. *Chin. J. Polym. Sci.* **2012**, *30*, 853.
14. Liu, B.; Shangguan, Y.; Song, Y.; Zheng, Q. *J. Appl. Polym. Sci.* **2013**, *129*, 973.
15. Park, J. U.; Kim, J. L.; Kim, D. H.; Ahn, K. H.; Lee, S. J.; Cho, K. S. *Macromol. Res.* **2006**, *14*, 318.
16. Lee, H. S.; Cho, E.; Ryoun Youn, J. *J. Appl. Polym. Sci.* **2007**, *103*, 3506.
17. Bhattacharya, S.; Gupta, R. K.; Jollands, M.; Bhattacharya, S. N. *Polym. Eng. Sci.* **2009**, *49*, 2070.
18. Botta, L.; Scaffaro, R.; La Mantia, F. P.; Dintcheva, N. T. *J. Polym. Sci. Part B: Polym. Phys.* **2010**, *48*, 344.
19. Li, Q.; Yang, Q.; Huang, Y.; Chen, G.; Lv, Y. *J. Macromol. Sci. B* **2012**, *51*, 1776.
20. Laguna-Gutierrez, E.; Lopez-Gil, A.; Saiz-Arroyo, C.; Van Hooghten, R.; Moldenaers, P.; Rodríguez-Perez, M. A. *J. Polym. Res.* **2016**, *23*, 251.
21. Rohlmann, C. O.; Horst, M. F.; Quinzani, L. M.; Failla, M. D. *Eur. Polym. J.* **2008**, *44*, 2749.
22. Riechert, V.; Failla, M. D.; Quinzani, L. M. *J. Thermoplast. Compos.* **2016**, *30*, 741.
23. Cole, K. C. *Macromolecules* **2008**, *41*, 834.
24. Százdi, L.; Pukánszky, B., Jr.; Földes, E.; Pukánszky, B. *Polymer* **2005**, *46*, 8001.
25. Rohlmann, C. O.; Failla, M. D.; Quinzani, L. M. *Polymer* **2006**, *47*, 7795.
26. Horst, M. F.; Quinzani, L. M.; Failla, M. D. *J. Thermoplast. Compos.* **2014**, *27*, 106.
27. Durmus, A.; Kasgoz, A.; Macosko, C. W. *Polymer* **2007**, *48*, 4492.
28. Devendra, R.; Hatzikiriakos, S. G.; Vogel, R. *J. Rheol.* **2006**, *50*, 415.
29. Tang, Y.; Yang, C.; Gao, P.; Ye, L.; Zhao, C.; Lin, W. *Polym. Eng. Sci.* **2011**, *51*, 133.
30. Galgali, G.; Ramesh, C.; Lele, A. *Macromolecules* **2001**, *34*, 852.
31. Gu, S. Y.; Ren, J.; Wang, Q. F. *J. Appl. Polym. Sci.* **2004**, *91*, 2427.
32. Lertwimolnun, W.; Vergnes, V. *Polymer* **2005**, *46*, 3462.
33. Treece, M. A.; Oberhause, J. P. *Macromolecules* **2007**, *40*, 571.
34. Ren, J.; Silva, A. S.; Krishnamoorti, R. *Macromolecules* **2000**, *33*, 3739.
35. Sepehr, M.; Utracki, L. A.; Zheng, X.; Wilkie, C. A. *Polymer* **2005**, *46*, 11569.
36. Gahleitner, M. *Prog. Polym. Sci.* **2001**, *26*, 895.
37. Mittal, V. *J. Appl. Polym. Sci.* **2008**, *107*, 1350.
38. Pannirselvam, M.; Genovese, A.; Jollands, M. C.; Bhattacharya, S. N.; Shanks, R. A. *eXPRESS Polym. Lett.* **2008**, *2*, 429.
39. Horst, M. F.; Tuckart, W.; Del Blanco, L.; Failla, M. D.; Quinzani, L. M. *J. Appl. Polym. Sci.* **2012**, *125*, E495.
40. Choudalakis, G.; Gotsis, A. D. *Eur. Polym. J.* **2009**, *45*, 967.
41. Zhu, S.; Chen, J.; Zuo, Y.; Li, H.; Cao, Y. *Appl. Clay Sci.* **2011**, *52*, 171.
42. Decker, J. J.; Meyers, D. R.; Schiraldi, D. A.; Hiltner, A.; Nazarenko, S. *Polymer* **2015**, *61*, 42.
43. Mirzadeh, A.; Kokabi, M. *Eur. Polym. J.* **2007**, *43*, 3757.
44. Sanguansat, P.; Amornsakchai, T. *J. Polym. Res.* **2015**, *22*, 1.
45. Khalaj, M. J.; Ahmadi, H.; Lesankhosh, R.; Khalaj, G. *Trends Food Sci. Technol.* **2016**, *51*, 41.